High Temperature Corrosion of Materials (2024) 101:897–909
https://doi.org/10.1007/s11085-024-10285-4

ORIGINAL PAPER

Reaction of a Molten Cr-Si-Base Alloy with Ceramics and a High Entropy Oxide

Lucas Pelchen[1] · Manuel Schenker[2] · Maren Lepple[2] · Anke Silvia Ulrich[1]

Received: 17 July 2024 / Revised: 17 July 2024 / Accepted: 22 July 2024 /
Published online: 8 August 2024

Abstract

Due to their higher thermal and chemical stability than other high-temperature materials, chromium-silicon-base (Cr-Si-base) alloys are promising materials for future gas turbines and other high-temperature applications operating under harsh conditions. To enable near-net-shape casting of Cr-Si-base alloys, a compatibility of the alloy melt with the ceramic crucibles and molds is necessary. Additionally, a metal-ceramic contact exists at the interface between thermal barrier coating (TBC) and alloy, where metallic may melts play a role in the case of coating failure and overheating. In this study, molten $Cr_{92}Si_8$ (in at. %) alloy is brought into contact with powders of ceramics commonly used for casting molds or crucibles (e.g. $ZrSiO_4$, Al_2O_3, 3YSZ), to investigate liquid metal corrosion, interdiffusion, and stabilities. Additionally, the high entropy oxide $(Sm_{0.2}Gd_{0.2}Dy_{0.2}Er_{0.2}Yb_{0.2})_2Zr_2O_7$ (HEO), a potential future TBC material, is investigated. Before melting using an electric arc furnace, the powders of the investigated ceramics were mixed with pulverized $Cr_{92}Si_8$ and pressed into alloy-ceramic pairs, to maximize the contact area between molten metal and ceramic. For microstructural investigations and phase analysis, the materials were assessed using scanning electron microscopy (SEM) equipped with energy-dispersive X-ray spectroscopy (EDS), and X-ray diffraction (XRD). The widely used mold material $ZrSiO_4$ and the coating BN were found to decompose, while reaction products of SiO_2 and $CoAl_2O_4$ with the melt were detected. Al_2O_3, 3YSZ, and the HEO did not show decomposition or corrosion by the melt. Al_2O_3, 3YSZ, and the HEO are therefore considered as promising crucible, mold, and TBC materials for Cr-Si-base alloys.

Keywords Chromium-Silicon-Base alloy · Liquid metal corrosion · High entropy oxide · Melt-Ceramic-Interaction

Extended author information available on the last page of the article

Introduction

Given the rising efficiency requirements for high-temperature applications, such as gas turbines, and the associated higher thermal loads on the materials used, Cr-Si-base alloys are promising structural materials. They are characterized by a binary microstructure consisting of chromium solid solution Cr_{ss} and A15 phase precipitates (Cr_3Si in the case of the binary composition). The precipitates result in a higher specific strength [1] and better oxidation and nitridation resistance [2] than commonly used Ni-base alloys. As for refractory metal alloys, for production of Cr-base alloys, mostly powder metallurgical processes [3, 4] or electric arc furnaces on a laboratory scale [2, 5, 6] are used to achieve low levels of impurities. For casting near-net-shape parts, such as turbine blades made from Ni-base superalloys, vacuum induction melting, and lost-wax investment casting are commonly used. In these processes, either an inductively heated crucible or an actively heated ceramic shell mold is in contact with liquid metal. The melt has a temperature higher than 1000 °C, and the mold is exposed to it for dwell times up to several hours. For Ni-base alloys, common mold materials are alumina (Al_2O_3) and zircon ($ZrSiO_4$), each in combination with a silica (SiO_2)-based binder system [7], all of which have decomposition or melting temperatures well above the melting point of Ni. However, a reaction of Ni-containing melt with these mold materials has been observed during the casting of single-crystalline Ni-base components [7]. Therefore, a barrier coating based on boron nitride (BN) [8] is used to reduce interfacial reactions. In addition, mold additives like cobalt aluminate ($CoAl_2O_4$) [9] are widely used. First studies focusing on the castability of Cr-Si-base alloys [10], reveal that investment casting is possible. However, the melt strongly interacts with the conventional mold systems, forming deep and numerous defects at the surface of the casting. A study from 1963 recommends the use of yttria-stabilized zirconia (3YSZ) crucibles for the casting of Cr-base alloys due to its thermal and chemical stability [11, 12]. Yttria-stabilized zirconia with a higher yttria content (7YSZ) is the state-of-the-art material for thermal barrier coatings (TBCs). TBCs are applied to metallic parts in gas turbines for thermal insulation and corrosion protection. Because the turbine blades can overheat despite the TBC and the blade material can melt locally [13], a possible melt contact is therefore considered in the TBC design. Thus, a promising future TBC material is added to this study: the high entropy oxide (HEO) $(Sm_{0.2}Gd_{0.2}Dy_{0.2}Er_{0.2}Yb_{0.2})_2Zr_2O_7$ with a defect fluorite structure. Defect fluorites like this do not show a phase transition up to 1500 °C and are potentially stable to 2700 °C [14, 15]. Currently, it is unclear which of the conventional mold systems components, binder (e.g. SiO_2), coating (e.g. BN), or a structural ceramic (e.g. $ZrSiO_4$), meets the required thermal stability and corrosion resistance in contact with molten Cr-Si-base alloys. Additionally, the feasibility of 3YSZ, mentioned in an over 60-year-old study must be revisited and further evaluated. Regarding the compatibility of molten Cr-Si-base alloy with HEO, no investigations have been conducted so far to the best of the authors' knowledge. In this study, the corrosion resistance and thermal stability of selected ceramics (Al_2O_3, $ZrSiO_4$,

SiO_2, $CoAl_2O_4$, BN, 3YSZ, and HEO) in contact with the melt of the Cr-Si-base alloy $Cr_{92}Si_8$ (composition in at. %) are investigated experimentally. The composition $Cr_{92}Si_8$ is most promising for casting as it contains a maximum amount of Si, leading to the formation of small, strengthening secondary A15-phase precipitates during heat treatment, while the formation of large primary A15 precipitates at the grain boundaries is suppressed [16]. By mixing the ceramic and metallic powders before melting, the interface area is maximized. The results of this study should lead to a better insight into stabilities of ceramics against liquid metal corrosion by molten Cr-Si-base alloys. Progress in defining suitable ceramics for casting molds, crucibles, and TBCs for alloys beyond Ni-base superalloys is expected.

Experimental Procedures

Powder Manufacturing

Cr-Si-base alloys with $Cr_{92}Si_8$ composition were manufactured from chromium pieces (Cr > 99.95 wt. %, HMW Hauner GmbH & Co. KG, Germany) and silicon granulate (Si > 99.999 wt. %, Thermo Fisher Scientific Inc., USA) using an electric arc furnace with 52 kPa argon 5.0. To ensure compositional homogeneity, the ingot was remelted five times. For reducing impurities, a zirconium getter was melted twice before melting the Cr-Si-base alloy. The 20 g $Cr_{92}Si_8$ ingots were ground to powder using a mono-planetary ball mill with balls and bowl made of tungsten carbide (WC). The commercially available ceramic powders used in this study are α-Al_2O_3 (99.78 wt. %, Alodur WSK F30, Munk + Schmitz Oberflächentechnik GmbH & Co. KG, Germany), $ZrSiO_4$ (65.9 wt. % ($ZrO_2 + HfO_2$) 32.1 wt. % SiO_2, MICROZIR Flour 200, CHILCHES MATERIALS, S.A., Spain), α-SiO_2 (> 99 wt. %, Microsil M500, Euroquarz GmbH, Germany), $CoAl_2O_4$ (> 99 wt. %, Cobalt Aluminate, Ransom & Randolph, USA), BN (> 98.5 wt. %, HeBoFill SP 010, Henze BNP AG, Germany), and 3YSZ (> 94.3 wt. % ZrO_2, 5.4 wt. % Y_2O_3, CY3Z-RS, SEPR – SAINT-GOBAIN ZIRPRO, France). The HEO was manufactured via the reverse co-precipitation route described by Hutterer and Lepple [14]. For the synthesis, 0.12 M solutions were prepared by dissolving following salts (Sigma-Aldrich Chemie GmbH, Germany) in deionized water: $Sm(NO_3)_3 \cdot 6\ H_2O$, $Gd(NO_3)_3 \cdot 6\ H_2O$, $Dy(NO_3)_3 \cdot 6\ H_2O$, $Er(NO_3)_3 \cdot 5\ H_2O$ all with a purity of 99.9 wt. %, apart from $Yb(NO_3)_3 \cdot 5\ H_2O$ (99 wt. %,), and $ZrOCl_2 \cdot 8\ H_2O$ (98 wt. %,). The final concentration of the solutions was determined gravimetrically. The stoichiometric mixtures were added dropwise in an ammonia solution with pH ≈ 10 to precipitate the respective metal cation hydroxides. The pH value was kept constant during the reaction by the addition of further ammonia solution. The hydroxides were filtered, washed, and dried at 80 °C. Subsequently, they were pressed into 13 mm pellets (4 t for 10 min). The pellets were then calcinated on Pt-sheets in an alumina crucible for 100 h at 1500 °C before grinding down to powder.

Metallic Melt and Ceramic Interaction Experiments

1 g of ceramic powder and 5 g of $Cr_{92}Si_8$-alloy powder were mixed and pressed into pellets (Ø 16 mm × 10 mm) using a pressure of 20 MPa for 2 min. The pellets were transferred to the electric arc furnace and melting was conducted as described above for alloy manufacturing but with remelted six times. During this procedure, the ceramic was in contact with the melt for around 2 min. In the following, these samples are referred to as alloy-ceramic pairs or $Cr_{92}Si_8$/ceramic.

Metallographic Preparation and Microstructural Analysis

The D_{50} particle sizes of the alloy and ceramic powders were measured using a laser granulometer (PSA 1190; Anton Paar GmbH, Germany). The alloy powder composition was measured using scanning electron microscopy and energy-dispersive X-ray spectroscopical analysis SEM/EDS (1540 EsB Cross Beam, Carl Zeiss AG, Germany/ UltraDry 30 mm^2 Detector; Thermo Fisher Scientific Inc., Germany). The alloy-ceramic pairs were hot mounted and ground to a final surface finish of 1 µm using SiC paper and diamond suspension. Optical microscopy, qualitative, and quantitative SEM/EDS measurements were used to investigate the samples' homogeneity and elemental distribution. To evaluate the porosity, the area fraction of pores of either five binarized backscattered electron (BSE) images ($Cr_{92}Si_8$ with $ZrSiO_4$, BN, 3YSZ, or HEO) or four binarized elemental distribution maps ($Cr_{92}Si_8$ with Al_2O_3, SiO_2, or $CoAl_2O_4$), depending on the contrast between pores and ceramic in BSE, were measured. Phase analysis was done using X-ray diffraction (XRD) measurements (Bruker D8 Advance, USA) with monochromatic Cu-K_α radiation.

Results

Investigations of Powders

Information on phase compositions, measured particle sizes, decomposition, and melting temperatures of the used powders are listed in Table 1. According to the XRD the $Cr_{92}Si_8$ powder consists of Cr_{SS} and Cr_3Si phase. Impurities of 0.3 at. % tungsten and carbon were measured using SEM/EDS and attributed to contaminations during milling. Using XRD on the purchased ceramics could verify their crystal structure: α-Al_2O_3, $ZrSiO_4$, α-SiO_2, $CoAl_2O_4$, and hexagonal (h-) BN. In case of the HEO only peaks of the defect fluorite phase were detected confirming the phase purity. For 3YSZ, a tetragonal (t-)ZrO_2 ($P4_2/nmc$) phase and a monoclinic (m-)ZrO_2 ($P2_1/a$) phase were detected.

Table 1 Overview of particle size, phase composition, and melting or decomposition temperatures of the used powders. The melting temperatures are marked with*, and decomposition temperatures with[x]

Name	Phases (space group)	Temperatures in °C	Particle size D_{50} in µm
$Cr_{92}Si_8$	Cr_{ss} (Im $\bar{3}$ m) and Cr_3Si (Pm $\bar{3}$ n)	*1807 [17]	45.8 ± 7.7
Al_2O_3	α-Al_2O_3 (R $\bar{3}$ c)	*2045 [18]	594.1 ± 158.1
$ZrSiO_4$	$ZrSiO_4$ ($I4_1$/amd)	[x]1635: α-SiO_2 and ZrO_2 [19], *ZrO_2: 2708 [19]	18.7 ± 5.7
SiO_2	α-SiO_2 ($P3_221$)	*1726 [20]	3.6 ± 0.9
$CoAl_2O_4$	$CoAl_2O_4$ (Fd $\bar{3}$ m)	1980 [21]	6.4 ± 1.7
BN	h-BN (P $\bar{3}$ m1)	[x] > 1400: B and N_2 [22], *2397 [23]	0.9 ± 0.2
3YSZ	t- ZrO_2 ($P4_2$/nmc) and m-ZrO_2 ($P2_1$/a)	*2720 [24]	0.1 ± 0.1
HEO	$(Sm_{0.2}Gd_{0.2}Dy_{0.2}Er_{0.2}Yb_{0.2})_2$ Zr_2O_7 (Fm $\bar{3}$ m)	* > 2700 [14]	10.5 ± 2.9

Porosities Formed in Alloy-Ceramic Pairs

In Table 2, the measured area fractions of pores are shown for the different alloy-ceramic pairs. The $Cr_{92}Si_8$/BN pair, followed by the $Cr_{92}Si_8$/$ZrSiO_4$ pair, exhibited a significantly higher porosity than the other combinations. The smallest pore area fractions were found in the pairs containing Al_2O_3 and $CoAl_2O_4$. In the case of Al_2O_3, $CoAl_2O_4$, SiO_2, $ZrSiO_4$, and BN, the measured porosity is mainly located in the metallic phase or at the metal/ceramic interface, whereas for the pairs with 3YSZ and HEO the majority of pores could be found inside the ceramic.

$Cr_{92}Si_8$/Ceramic Interfaces

Unstable Alloy-Ceramic Pairs.

In Fig. 1, representative images of interfaces of SiO_2 and $Cr_{92}Si_8$ melt after cooling are shown. A Cr_{ss} matrix and Cr_3Si precipitates were found beside ceramic particles. The smaller particles (SP), consisting of Cr, Si, and O, showed a significantly higher Cr concentration of 58 at. % as the larger particle (LP). LP in contrast showed significant inhomogeneities in EDS elemental maps, which is why two compositions were distinguishable (LP-1 and LP-2). LP-1, at the Cr_{SS}/particle interface and in the particle core had a 14 at. % higher Cr and 17 at. % lower O concentration compared to LP-2 in the rest of the particle. In addition, the Cr_{SS} phase contained 12 at. % Si instead of the original 8 at. % Si, confirming an enrichment with Si. Besides Cr_{SS} and Cr_3Si, only α-SiO_2 ($P3_221$) was detected using XRD measurements (not shown here). Investigations of several ceramic particles of different sizes showed, that Cr accumulated in SiO_2 to an average depth of 23 ± 5 µm surrounding a SiO_2 core.

In Fig. 2 the microstructure of the $Cr_{92}Si_8$/BN pair is shown. Besides the Cr_{ss} matrix and Cr_3Si phase, pores, B- and N-enriched phases were revealed by EDS and XRD measurement, but no hints of remaining BN were detected (see Fig. 2b–e)

Table 2 Overview over pore area fraction of the melted alloy-ceramic samples investigated

Alloy-ceramic pair	$C_{92}Si_8/Al_2O_3$	$C_{92}Si_8/CoAl_2O_4$	$C_{92}Si_8/SiO_2$	$C_{92}Si_8$/HEO	$C_{92}Si_8$/3YSZ	$C_{92}Si_8/ZrSiO_4$	$C_{92}Si_8$/BN
Pore area fraction in %	0.1 ± 0.1	0.1 ± 0.1	0.3 ± 0.4	1.0 ± 1.7	2.0 ± 0.7	5.4 ± 8.7	11.2 ± 14.7

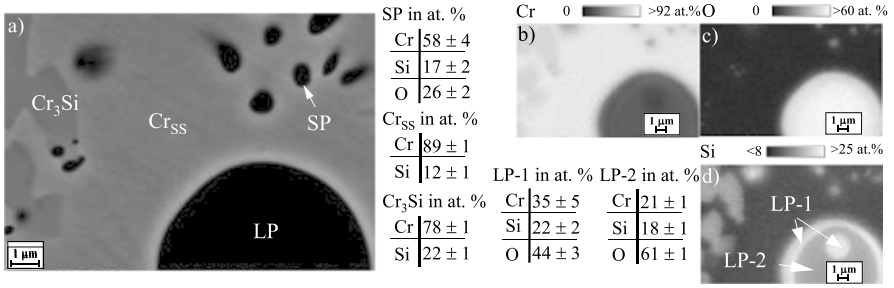

Fig. 1 BSE image of the cross section of the $Cr_{92}Si_8/SiO_2$ pair showing small (SP) and large particles (LP) with quantitative EDS spot measurements (**a**) and corresponding elemental distribution maps (**b–d**)

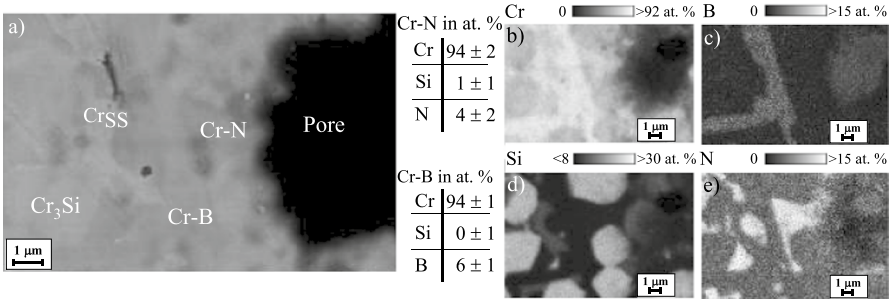

Fig. 2 **a** BSE image of $Cr_{92}Si_8$/BN microstructure with quantitative EDS measurements of the nitride and boride phases **b–e** element distribution maps

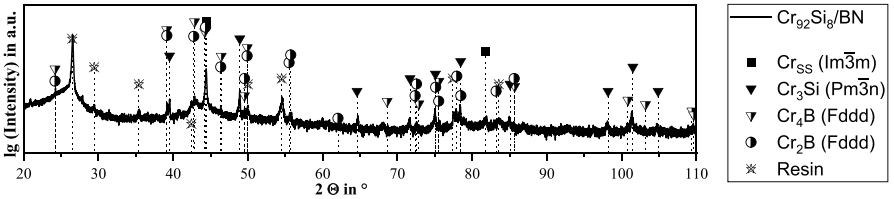

Fig. 3 XRD pattern of the $Cr_{92}Si_8$/BN pair

and Fig. 3). The negligible number of other elements despite Cr in these areas leads to the assumption that Cr–N and Cr-B phases formed during arc melting while BN decomposed. The nitride phase could not be detected using XRD but based on the binary Cr–N phase diagram [25], most probably, Cr_2N formed.

In Fig. 4 two representative areas of the $Cr_{92}Si_8/CoAl_2O_4$ pair are shown. In areas, where the area fraction of the ceramic significantly exceeds that of the alloy (see Fig. 4a)), a Co-enriched Cr_{ss} matrix with 13 at. % Co and SiO_2 precipitates formed instead of the original Cr_{ss} and Cr_3Si microstructure (see Fig. 4a, c–g). At the alloy/ceramic interface, a Cr-Co-Si–O phase formed, which has a high Cr content of 84 at. % and appears to be a single phase with respect to the SEM resolution. On

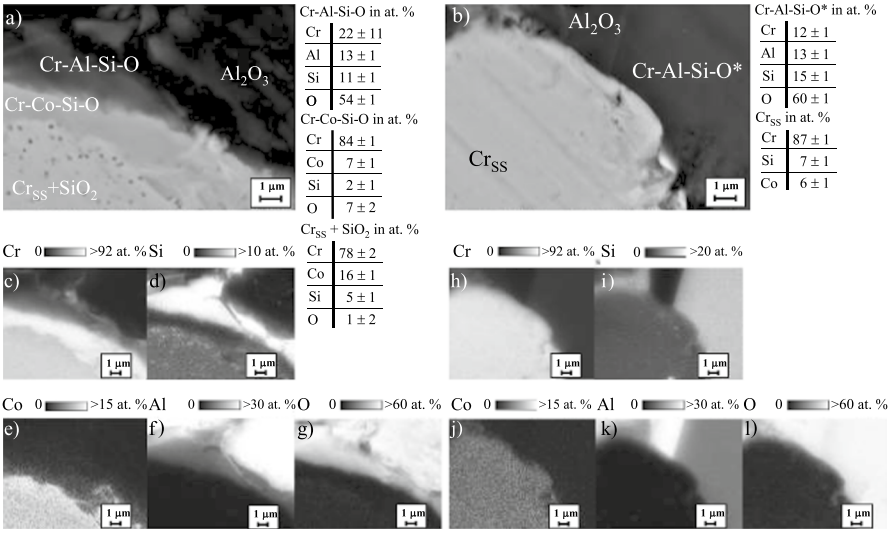

Fig. 4 BSE images and EDS element maps **a**, **c–g** of a representative area with a higher metallic fraction and **b**, **h–l** of a representative area with higher ceramic fraction. The alloy-ceramic pair is $Cr_{92}Si_8$/$CoAl_2O_4$. Quantitative EDS measurements of selected phases are added

the other hand, in areas where the proportion of $Cr_{92}Si_8$ predominates (see Fig. 4b), Cr_{ss} with higher Si concentration and lower Co concentration formed (see Fig. 4b, h–l). No oxygen was detected in these areas with respect to the method's measurement uncertainties. In both areas, Al_2O_3 and Cr-Al-Si–O phases were detected. This Cr-Al-Si–O phase had a 10 at. % higher Cr concentration in the areas with a higher ceramic fraction compared to Cr-Al-Si–O* in the alloy-rich regions. XRD analysis of the sample (not shown here) confirmed the presence of Al_2O_3 (R $\bar{3}$ c), SiO_2 ($P3_221$), and Co-enriched Cr_{SS} (Im $\bar{3}$ m), but no other phases were detected.

Figure 5, the cross section of $Cr_{92}Si_8/ZrSiO_4$ is shown, as well as the XRD patterns of the $ZrSiO_4$ pow-der and the $Cr_{92}Si_8/ZrSiO_4$ pair. $ZrSiO_4$ is found to be unstable in contact with $Cr_{92}Si_8$ melt. In the BSE image, black areas at the ZrO_2/Cr_{SS} interface are found which are attributed to glassy SiO2 and pore formation comparable to the findings by Kaiser et al. [26]. Si-enrichments in the

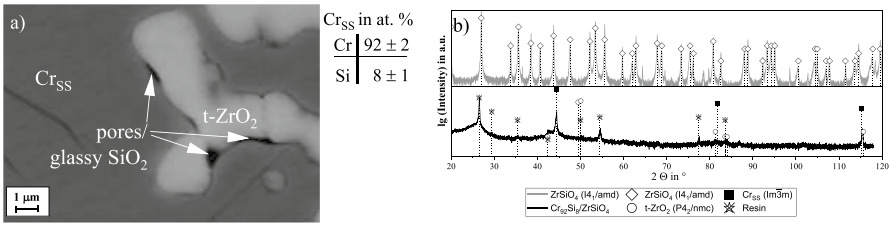

Fig. 5 **a** BSE image of the $Cr_{92}Si_8/ZrSiO_4$ pair and **b** XRD-pattern of the $ZrSiO_4$ powder and the $Cr_{92}Si_8$/$ZrSiO_4$ pair

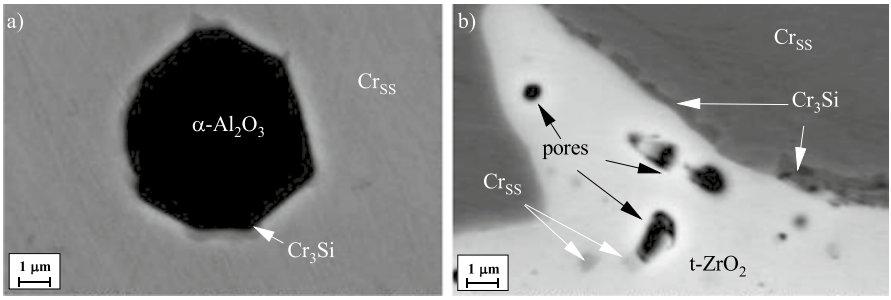

Fig. 6 BSE image of **a** $Cr_{92}Si_8/Al_2O_3$ pair microstructure and **b** $Cr_{92}Si_8$/3YSZ microstructure

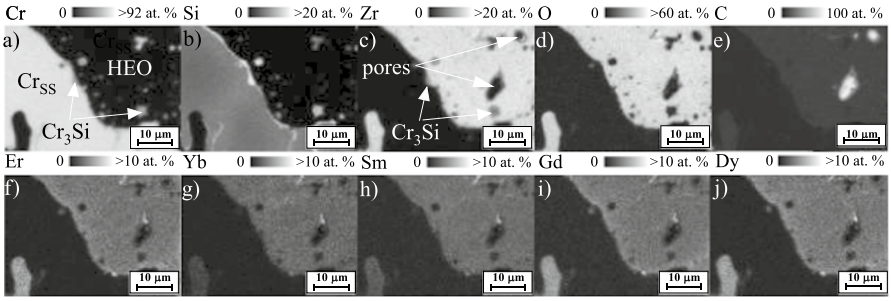

Fig. 7 **a–j** Element distribution EDS maps of $Cr_{92}Si_8$/HEO after melt contact

interface region were detected using EDS, and pores were detected by tilting the sample and using SE-mode (SEM) to see differences in depth. The ratio of the area fraction of black phase to t-ZrO_2 was measured using image analysis and is 0.08—0.12. $ZrSiO_4$ was not detected after arc melting neither with SEM/EDS nor XRD. Instead, both measurements revealed only the presence of t-ZrO_2, Cr_{SS}, and Cr_3Si.

Stable Alloy-Ceramic Pairs.

As shown in Fig. 6 Al_2O_3 and 3YSZ showed no additional phase formation nor decomposition in contact with the $Cr_{92}Si_8$ melt. In both cases, the only phase observed at the ceramic/alloy interface was Cr_3Si. Even if 3YSZ showed pores inside the ceramic, no interdiffusion or phase formation was observed. XRD measurements confirmed, that for $Cr_{92}Si_8/Al_2O_3$ and for $Cr_{92}Si_8$/3YSZ no phases besides Cr_{SS}, Cr_3Si, and the corresponding ceramic phase Al_2O_3 ($R\bar{3}c$) or t-ZrO_2 ($P4_2/nmc$) formed.

As shown in Fig. 7, only Cr_3Si phase formation occurred at the HEO/$Cr_{92}Si_8$ interface. Beside this, inhomogeneities were detected inside the ceramic. These inhomogeneities are enriched in Cr, Si, or C and show low amounts of Zr, O, or the rare earth metals used in the ceramic. It is presumed, that these inhomogeneities are pores of the ceramic occurred during synthesis or processing, which were filled with Cr-Si-base melt during casting or resin during preparation. No signs for interdiffusion, reaction or corrosion of the ceramic by the metal melt were observed nor

decomposition. XRD results (not shown here) revealed the presence of peaks of the defect fluorite besides the Cr_{SS} and Cr_3Si.

Discussion

Al_2O_3, 3YSZ, and $(Sm_{0.2}Gd_{0.2}Dy_{0.2}\ Er_{0.2}Yb_{0.2})_2Zr_2O_7$ did not show any decomposition or corrosion products when contacted by the metallic melt in contrary to SiO_2, $CoAl_2O_4$, BN, and $ZrSiO_4$. Since the melting temperature of $Cr_{92}Si_8$ exceeds the decomposition temperature of BN and $ZrSiO_4$ (see Table 1), none of the original phases could be detected after melt contact, neither with EDS nor XRD. The decomposition of BN was confirmed by local nitride and Cr_4B formation (see Fig. 2). Beside nitride formation, gaseous species formed during arc melting of $Cr_{92}Si_8$/BN leading to an increased porosity (see Table 2). During the arc-melting process and, therefore, during gas formation, the oxygen partial pressure, $p(O_2)$, was low. Hence, the dominating gaseous species is assumed to be $N_{2(g)}$. Decomposition was also confirmed for $ZrSiO_4$ by detection of t-ZrO_2 and areas appearing black in the BSE image, which are attributed to SiO_2 and pore formation (Fig. 5). This is comparable to an earlier study on the thermal stability of $ZrSiO_4$ [26]. The detected Si-enrichment is limited to small areas (< 1 µm) at the Cr_{SS}/ZrO_2 interface, and the area fraction determined for black areas/t-ZrO_2 is 0.08—0.12. This is less than the ratio observed by Kaiser et al. [26] (0.74—1.49) and does not fit to the 32.1 wt. % SiO_2 in $ZrSiO_4$. Because of the low $p(O_2)$ during melting an explanation is the formation of volatile SiO(g) which previously has been observed for Si-SiO_2 systems [27]. The extensive formation of pores found in the $Cr_{92}Si_8$/BN and $Cr_{92}Si_8/ZrSiO_4$ pairs are in good agreement with the high amount of surface defects reported in a recent study on investment casting of Cr-Si-base alloys by Sandner et al. [10]. In contrast to the findings on $Cr_{92}Si_8/ZrSiO_4$, Si-rich oxides are present in the $Cr_{92}Si_8/SiO_2$ pair after fabrication. The large particles in Fig. 1 are in the range of the powder size (compare Table 1). However, much larger SiO_2-particles were found due to the melting of SiO_2 during arc melting. The Si-enrichment of the Cr_{SS} up to the solution limit of around 12 at. % at the eutectic temperature [17] confirms the diffusion of Si into Cr_{SS}. As shown in Table 2, a very low area fraction of pores is detected. As SiO_2, contrary to $ZrSiO_4$, does not decompose into a solid and a liquid phase but melts below the alloy melting point (compare Table 1) the surface tension effect could counteract pore formation. The diffusion of Cr into SiO_2, declared as very strong by other researchers [14, 28, 29], is also observed in this study, and probably further intensified on contact with liquid SiO_2. The enrichment of Cr_{SS} with Si and that of SiO_2 with Cr (see Fig. 1) without forming other phases is evidence of interdiffusion between the alloy and SiO_2. The mechanism of Si-enrichment in Cr_{ss} when in contact with liquid SiO_2 was not investigated in detail in this study and needs further investigations. For $CoAl_2O_4$, a higher melting temperature compared to $Cr_{92}Si_8$ is reported [21]. However, the formation of Al_2O_2 and a Cr-, Al-, and Si-rich oxide or oxides, and Co-enriched Cr_{SS} with SiO_2 precipitates were found. For $CoAl_2O_4$ in molds for Cr-enriched Ni-base alloys, Co was found to diffuse into the Ni alloy. The formation of Cr_2O_3, Al_2O_3, and Co lead Binczyk et al. to the assumption of a

Table 3 Overview of stability of ceramics in contact with molten $Cr_{92}Si_8$. The resistance is categorized in no (-), small (○), and strong (+)

Ceramic	SiO_2	BN	$CoAl_2O_4$	$ZrSiO_4$	Al_2O_3	3YSZ	$(Sm_{0.2}Gd_{0.2}Dy_{0.2}Er_{0.2}Yb_{0.2})_2Zr_2O_7$
Stability	-	-	-	-	+	+	+

$CoAl_2O_4$-decomposition [30]. In this study, the enrichment of the Cr-phases with Co is comparable, however, SiO_2 is formed instead of Cr_2O_3 due to its higher thermodynamic stability. Due to phase decompositions, liquid melt corrosion accompanied by interdiffusion or reaction phase formation, and the formation of gaseous species, BN, SiO_2, $ZrSiO_4$, and $CoAl_2O_4$ are considered unsuitable as mold materials for the casting of Cr-Si-base alloys. Al_2O_3, HEO, and 3YSZ proved to be sufficiently thermally and chemically stable in contact with $Cr_{92}Si_8$ melt with respect to the conducted experiments. This is confirmed by the thermodynamic stabilities of Al_2O_3 and t-ZrO_2, which are higher than that of Cr_2O_3. 3YSZ fully transforms to t-ZrO_2, which seems to have a neglectable influence on the chemical stability, proving the findings of Sims [12]. Hence, neither EDS nor XRD, reveal sights of reaction or decomposition phases. Thus, also the HEO was found to be stable in contact with $Cr_{92}Si_8$ melt. The increased pore area fraction of 3YSZ and HEO compared to Al_2O_3 is attributed to the porosity of the ceramic particles in their initial state (see Fig. 6b) and Fig. 7). The findings regarding thermal and chemical stability of Al_2O_3, ZrO_2, and HEO from this study provide a suitable basis for further investigations regarding longer dwell times at elevated temperatures to mimic melt-ceramic contacts of several hours during investment casting or overheating in gas turbines.

Conclusion

In summary, Al_2O_3, 3YSZ, and $(Sm_{0.2}Gd_{0.2}Dy_{0.2}\ Er_{0.2}Yb_{0.2})_2Zr_2O_7$ are promising ceramics to be used in contact with molten Cr-rich Cr-Si-base alloys. Commonly used mold materials for casting Ni-base alloys such as SiO_2, $ZrSiO_4$, BN, and $CoAl_2O_4$ are not suitable for $Cr_{92}Si_8$ melt due to a lack of thermal stability and liquid metal corrosion. The corrosion resistance and temperature stability of the different ceramics in contact with molten $Cr_{92}Si_8$ are ranked in Table 3. Based on the comparable performance of Al_2O_3, 3YSZ, and $(Sm_{0.2}Gd_{0.2}Dy_{0.2}\ Er_{0.2}Yb_{0.2})_2Zr_2O_7$ reported in this study, 3YSZ and Al_2O_3 are mostly recommended as mold material or crucibles for lost-wax investment casting of Cr-Si-base alloys, due to the significantly lower price. HEO is considered as promising TBC material.

Acknowledgements The framework for this study is the MaDeRaisE project in the aviation research program LuFo VI-3 of the Federal Ministry for Economic Affairs and Climate Action listed under project number 20E2222. The authors thank the experimental support of Petra Pfizenmaier, Tobias Hardung, and Konstantin Müller from Metals and Alloys (II), University of Bayreuth, and Sven Scheler from Ceramic Materials Engineering, University of Bayreuth.

Author Contributions L.P. collected the data presented in the study and wrote the original manuscript draft, where M.S. and M.L. contributed the parts of the introduction and the materials and methods focussing on the high entropy oxides. A.U. and M.L. did the conceptualisation, funding acquisition and resources. A.U., M.L., M.S. and L.P. interpreted the data and worked on the visualisation. All authors reviewed and edited the manuscript.

Funding Open Access funding enabled and organized by Projekt DEAL.

Data Availability No datasets were generated or analyzed during the current study.

Declarations

Conflict of interest The authors declare that they have no known competing financial interests or personal relationships that could have appeared to influence the work reported in this paper.

References

1. A. Yuki, O. Toshihiro, and K. Ryosuke, *Intermetallics* **112**, 2019 (106526).
2. Soleimani-Dorcheh A., Mathias C. Galetz. Oxidation of Metals 2015; 84: 73.
3. R. Eck, H. P. Martinz, T. Sakaki, et al., *Materials Science and Engineering: A* **120**, 1989 (307).
4. U. Holzwarth and H. Stamm, *Journal of Nuclear Materials* **300**, 2002 (161).
5. A. S. Ulrich, P. Pfizenmaier, A. Solimani, et al., *Corrosion Science* **165**, 2020 (108376).
6. D. Teretyev, T. Khvan, J.-H. You, et al., *Journal of Nuclear Materials* **536**, 2020 (152204).
7. G. Brewster, N. D'Souza, K. S. Ryder, et al., *Metallurgical and Materials Transactions A* **4**, 2012 (1288).
8. F. Li, X. Chen, Y. Zhao, et al., *The International Journal of Advanced Manufacturing Technology* **5–8**, 2018 (1771).
9. Ł Rakczy, M. Grudzień, R. Cygan, et al., *Archives of Metallurgy and Materials* **63**, 2018 (1537).
10. Sandner, K., Völkl, R., Yeh, AC., et al. Int. J. Met. July 2024.
11. Y. I. Folomeikin, F. N. Karachevtsev, and V. L. Stolyarova, *Russian Journal of Inorganic Chemistry* **7**, 2019 (934).
12. C. T. Sims, *JOM* **2**, 1963 (127).
13. Guo, X., Zheng, W., Xiao, C., et al. Evaluation of microstructural degradation in a failed gas turbine blade due to overheating. Eng Fail Anal 2019; 209
14. P. Hutterer and M. Lepple, *Journal of the American Ceramic Society* **2**, 2023 (1547).
15. C. M. Rost, E. Sachet, T. Borman, et al., *Nat Commun* **6**, 2015 (8485).
16. A. S. Ulrich, P. Pfizenmaier, A. Solimani, et al., *Int J Refract Hard Met* **76**, 2018 (72).
17. I. Kazushige, A. Yuki, X. Xiao, et al., *Journal of Phase Equilibria and Diffusion* **43**, 2022 (229).
18. S. J. Schneider and C. L. McDaniel, *Journal of Research of the National Bureau of Standards Section A: Physics and Chemistry* **4**, 1967 (317).
19. Ball, R., Mignanelli, M. A., Barry, T. I., et al. Journal of Nuclear Materials 1993; 238
20. Ringdalen, E., Tangstad, M. MOLTEN16 2016; 43
21. J. Azuria, J. Marchal, and R. M. Laine, *Journal American Ceramic Society* **9**, 2006 (2749).
22. L. H. Dreger, V. V. Dadape, and J. L. Margrave, *The Journal of Physical Chemistry* **8**, 1962 (1556).
23. H. Okamoto, *Journal of Phase Equilibria* **2**, 2000 (208).
24. H. G. Scott, *Journal of Materials Science* **9**, 1975 (1527).
25. Ivanchenko, V.G., Mel'nichenko T.V Phys. Met. 1992; 11: 150

26. A. Kaiser, M. Lobert, and R. Telle, *Journal of the European Ceramic Society* **11**, 2008 (2199).
27. Y. Takakuwa, M. Nihei, T. Horie, et al., *Journal of Non-Crystalline Solids* **179**, 1994 (345).
28. K. Saga, R. Ohno, D. Shibata, et al., *ECS Journal of Solid State Science and Technology* **5**, 2015 (131).
29. X. Wang, K. Xue, C. Xu, et al., *Journal of Chemical Research* **5**, 2022 (174751982211312).
30. F. Binczyk, J. Sleziona, and P. Gradon, *Composites* **11**, 2011 (49).

Authors and Affiliations

Lucas Pelchen[1] · Manuel Schenker[2] · Maren Lepple[2] · Anke Silvia Ulrich[1]

✉ Anke Silvia Ulrich
silvia.ulrich@uni-bayreuth.de

[1] Metals and Alloys II, Faculty of Engineering Science, University of Bayreuth, Prof.-Rüdiger-Bormann-Str. 1, 95447 Bayreuth, Germany

[2] Institute of Inorganic and Analytical Chemistry, Justus Liebig University Giessen, Heinrich-Buff-Ring 17, 35392 Giessen, Germany